Proceedings of the International Conference of Control, Dynamic Systems, and Robotics
Ottawa, Ontario, Canada, May 15-16 2014
Paper No. 117

Self-propulsion of Jointed Bodies Near a Wall in an Ideal Fluid

Michael J. Fairchild, Scott D. Kelly
University of North Carolina at Charlotte
9201 University City Blvd., Charlotte NC, 28262, U.S.A.
mjfairch@uncc.edu; scott.kelly@uncc.edu

Abstract - A model for the locomotion of simple mechanical devices comprising spheres linked by jointed rods undergoing cyclic shape changes in an ideal fluid near an infinite wall is investigated. Our analysis begins with a first-order approximation to the kinetic energy for a sphere near a wall, derived by (Milne-Thomson, 1968). Numerical simulations of Lagrange's equations are presented that demonstrate motion towards the wall for these swimmers. The presence of the wall breaks a symmetry, and this compensates for the isotropic, rather than asymmetric, added masses of the spheres. Evidence is presented that a geometric phase may be relevant, despite a highly nonlinear and asymmetric Lagrangian.

Keywords: Locomotion, ideal hydrodynamics, nonlinear systems, geometric phase.

1. Introduction

(Purcell, 1977) investigated hydrodynamic locomotion of microorganisms swimming in Stokes flow, stating what is now referred to as the "Scallop Theorem." This says that an isolated microorganism enjoying only one internal degree of freedom cannot swim when viscous forces dominate. An analogous result applies to an isolated swimmer in an infinite ideal fluid when the system is initially at rest; this analogy is a consequence of parallels in the mathematical structure of ideal flow and Stokes flow detailed in (Kelly et al., 2012)

The locomotion of swimmers with additional internal degrees of freedom has been studied extensively. For example, (Radford, 2003), (Kanso et al., 2005), and (Ross, 2006) each demonstrated that a planar swimmer comprising two or more links can propel itself in an ideal fluid through a combination of cyclic shape changes and added-mass effects, generating geometric phase relative to a connection on a principal bundle. Meanwhile, (Koiller et al., 1996) showed that a pair of scallops can exploit their hydrodynamic coupling in Stokes flow to propel themselves as a team in a mathematically analogous fashion.

This work considers the locomotion of swimmers comprising spheres and jointed rods in ideal flow near an infinite wall. It differs from previous work in two important ways. First, the added mass of a sphere — unlike that of an ellipse — is isotropic, so asymmetric added-mass effects are eliminated. Second, the presence of the wall breaks a symmetry that, under the assumptions made in this paper, would otherwise render impossible the locomotion of the swimmers considered here. The locomotion of the swimmers considered in this paper appears to be solely accounted for by wall effects.

2. Model and Kinematics

The left panel of Figure 1 depicts a sphere in an inviscid fluid near an infinite wall, the building block on which our articulated swimmers are modeled. The middle panel depicts a *scallop*, and the right panel depicts a *two-jointed scallop*. These are comprised of spheres and ideal rods and will be described in turn.

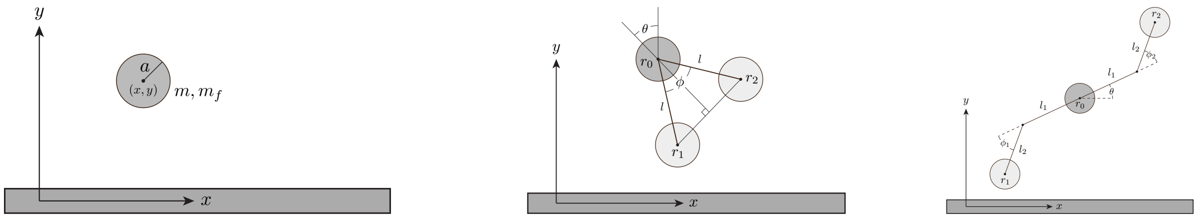

Fig. 1. A sphere near a wall (left); a scallop (middle); a two-jointed scallop (right)

2.1. Sphere in an Invisicid Fluid near a Wall

For the sphere near the wall, let a denote the radius, m the mass, and $r = (x, y)$ its position relative to an inertial frame fixed in the wall. Let m_f denote the mass of the displaced fluid. In §18.61 of (Milne-Thomson, 1968), a first-order approximation to the kinetic energy of the sphere is derived as

$$T := \tfrac{1}{2}(A(y)\dot{x}^2 + B(y)\dot{y}^2), \tag{1}$$

where

$$A(y) := m + \tfrac{1}{2}m_f(1 + \tfrac{3}{16}\tfrac{a^3}{y^3}), \tag{2}$$

$$B(y) := m + \tfrac{1}{2}m_f(1 + \tfrac{3}{8}\tfrac{a^3}{y^3}). \tag{3}$$

This result is obtained by solving Laplace's equation for the velocity potential subject to appropriate boundary conditions for the case of two spheres moving along their line of centers, and then using the method of images to obtain the result with a single sphere near an infinite wall. Note that the energy is independent of x, as it must be due to symmetry. Furthermore, it is highly nonlinear in y, and the vertical speed $\dot{y}$ is given more energetic weight than its horizontal counterpart $\dot{x}$. Furthermore, Milne-Thomson demonstrates that the sphere is

$$\text{repelled from the wall when } \dot{x}^2 - 2\dot{y}^2 < 0, \tag{4}$$

$$\text{attracted towards the wall when } \dot{x}^2 - 2\dot{y}^2 > 0. \tag{5}$$

2.2. Single-jointed Scallop as Three Spheres

The middle panel of Figure 1 depicts a scallop modeled by three spheres. Each sphere has radius a and mass m, and each displaces mass m_f of fluid. Relative to an inertial frame fixed in the nearby wall, the position of the central (or body) sphere is denoted r_0. The centers of the distal spheres are joined to the center of the body sphere by rigid, infinitesimally thin, massless rods of length $l \geq 2a$. Such a rod will henceforth be referred to as an *ideal rod*. These ideal rods do not interact with the fluid or make any contribution to the dynamics. The shape angle of the scallop, its *joint angle*, is denoted by ϕ. The *orientation* of the scallop, denoted θ, is defined to be zero when the vertical line through r_0 is the perpendicular bisector of the line segment joining r_1 to r_2. With $r_0(t) := (x(t), y(t))$, the geometry of Figure 1 implies that

$$x_1(t) = x(t) + l\sin(\theta(t) - \tfrac{\phi(t)}{2}), \tag{6}$$

$$y_1(t) = y(t) - l\cos(\theta(t) - \tfrac{\phi(t)}{2}), \tag{7}$$

$$x_2(t) = x(t) + l\sin(\theta(t) + \tfrac{\phi(t)}{2}), \tag{8}$$

$$y_2(t) = y(t) - l\cos(\theta(t) + \tfrac{\phi(t)}{2}). \tag{9}$$

As soon as l and the control $\phi(t)$ are prescribed, the motion of the system is completely determined by $x(t), y(t)$, and $\theta(t)$.

2.3. Two-jointed Scallop as Three Spheres

A more general swimmer, in which there are two joint angles, ϕ_1 and ϕ_2, is depicted in the right panel of Figure 1. With the aid of two — rather than one — shape variables, more sophisticated gaits may be studied. An ideal rod of length $2l_1$ passes through the center of the body sphere, making angle θ relative to the horizontal. Each end of this rod is attached via a swivel joint to another ideal rod of length l_2, the end of which is affixed at the center of the corresponding distal sphere. To permit the distal spheres to rotate freely while rendering collisions impossible, the parameters l_1 and l_2 are required to satisfy the inequalities

$$l_1 \geq 2a \quad \text{and} \quad a \leq l_2 \leq l_1 - 2a. \tag{10}$$

(Without these restrictions, the single-jointed scallop considered earlier is recovered as the special case $l_1 = 0$, in which case the single joint angle is $\phi = \pi - \phi_1 + \phi_2$.) With $r_0(t) := (x(t), y(t))$ as before, it follows from the geometry of Figure 1 that

$$x_1(t) = x(t) - l_1 \cos\theta(t) - l_2 \cos(\theta(t) + \phi_1(t)), \tag{11}$$
$$y_1(t) = y(t) - l_1 \sin\theta(t) - l_2 \sin(\theta(t) + \phi_1(t)), \tag{12}$$
$$x_2(t) = x(t) + l_1 \cos\theta(t) + l_2 \cos(\theta(t) + \phi_2(t)), \tag{13}$$
$$y_2(t) = y(t) + l_1 \sin\theta(t) + l_2 \sin(\theta(t) + \phi_2(t)), \tag{14}$$

and the motion of the system is completely determined by $x(t), y(t)$, and $\theta(t)$ once values for l_1, l_2 are specified and the controls $\phi_1(t)$ and $\phi_2(t)$ are prescribed.

3. Dynamics and Control

This work employs the *hydrodynamic decoupling assumption*, which says that interactions among the spheres are ignored; each sphere is treated as if its only interaction were with the wall.

3.1. Lagrangian Dynamics

Under the decoupling assumption, the Lagrangian $\mathscr{L}$ is the sum of the kinetic energies of the spheres,

$$\mathscr{L} = \sum_{i=0}^{2} \tfrac{1}{2}(A(y_i)\dot{x}_i^2 + B(y_i)\dot{y}_i^2), \tag{15}$$

and the dynamics are governed by Lagrange's equations,

$$\frac{d}{dt}\frac{\partial \mathscr{L}}{\partial \dot{q}^i} - \frac{\partial \mathscr{L}}{\partial q^i} = 0, \quad q := (x, y, \theta). \tag{16}$$

As is customary, let $p_x := \partial\mathscr{L}/\partial\dot{x}$, $p_y := \partial\mathscr{L}/\partial\dot{y}$, and $p_\theta := \partial\mathscr{L}/\partial\dot{\theta}$ denote the conjugate momenta induced by the Lagrangian. Since the Lagrangian is *cyclic* in x, i.e. $\partial\mathscr{L}/\partial x = 0$, the conjugate momentum p_x is conserved. In fact, its conservation serves as a useful check on the numerical integration of Lagrange's equations.

3.2. Control

The shape angles for both the scallop and two-jointed swimmer are prescribed by open-loop controls, the details of which are discussed in Section 4.

4. Numerical Simulation

With $\mathscr{L}$ given as in (15), and with the controls described in this section, Lagrange's equations (16) for both the single-jointed and two-jointed scallops were numerically simulated using Mathematica's `NDSolve` ODE solver. Initial velocities were determined programatically by requiring the vanishing of the system's net initial momentum. That is, $\dot{x}(0)$, $\dot{y}(0)$, and $\dot{\theta}(0)$ are found by requiring them to satisfy the system of equations

$$p_x(y,\theta,\dot{x},\dot{y},\dot{\theta}) = 0, \tag{17}$$

$$p_y(y,\theta,\dot{x},\dot{y},\dot{\theta}) = 0, \tag{18}$$

$$p_\theta(y,\theta,\dot{x},\dot{y},\dot{\theta}) = 0, \tag{19}$$

at $t = 0$, with $y = y_0$, and $\theta = \theta_0$. This ensures that any locomotion arises from the dynamics, rather than the initial conditions.

4.1. Single-Jointed Scallop

In the simulation m_f was chosen to be large relative to m (in particular, $m_f := 10m$) to ensure sufficient momentum transfer from the fluid to the scallop.[1] The scallop's joint is prescribed by the open-loop control

$$\phi(t) := \phi_{\min} + (\pi - \phi_{\min}) \cdot \tfrac{1+\sin t}{2}, \tag{20}$$

where $\phi_{\min} := 2\arcsin(\frac{a}{l})$ is the minimum physically-realizable joint angle, occuring when the distal spheres are tangent. This control produces sinusoidal motion of the joint angle, with a minimum value of $\phi_{\min}$ and a maximum value of π, where the joint is "wide open."

Figure 2 depicts the configuration of the scallop at equally spaced time intervals $t = 0, \frac{1}{3}t_{\max}, \frac{2}{3}t_{\max}, t_{\max}$. Comparison of the central sphere in the leftmost panel (at $t = 0$) with that in the rightmost panel (at $t = t_{\max}$) shows that the scallop has managed to inch its way towards the wall.

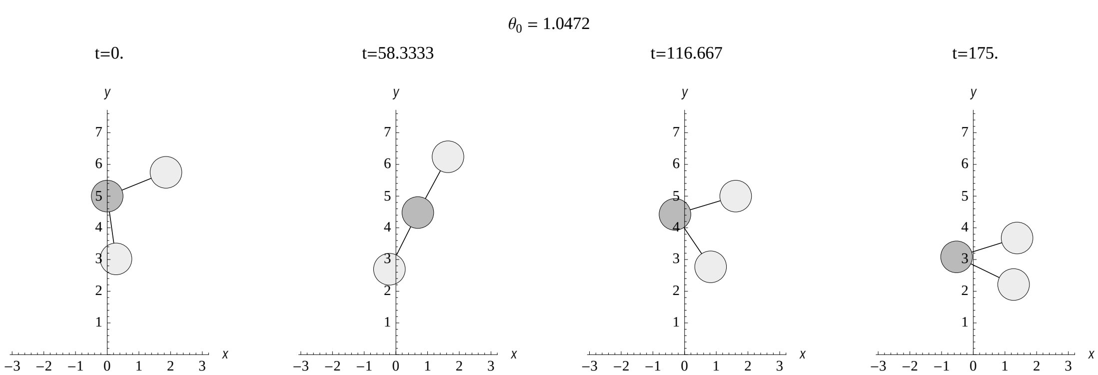

Fig. 2. Snapshots of scallop at equally spaced times

Figure 3 depicts the overall orientation of the scallop, revealing that the scallop is rotating, in the net, along its trajectory. This may also be seen in Figure 2, where the first panel shows the scallop in orientation $\pi/3$, and the last panel shows the scallop in orientation $\pi/2$ (approximately). Figure 4 depicts the trajectory of the central sphere of the scallop, which is seen to undergo a swinging motion. Although its x coordinate

[1] The full set of simulation parameters, or indeed the Mathematica notebooks, are available from the authors upon request.

oscillates, Figure 2 shows that this is balanced by oscillation of the distal spheres as well, so that the conjugate momentum p_x is conserved. Indeed, this is consistent — via Noether's theorem — with the fact that the system exhibits a translational symmetry along the x axis.

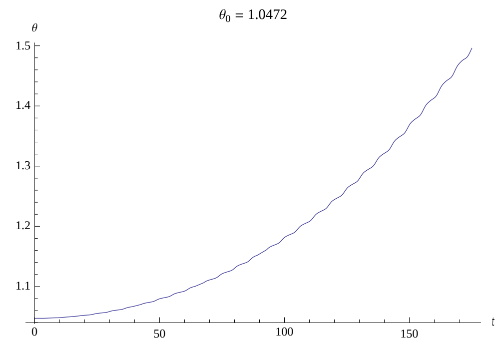

Fig. 3. Orientation of scallop

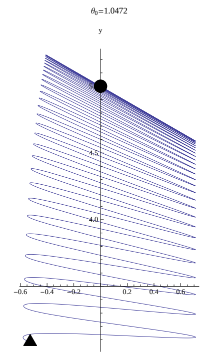

Fig. 4. Trajectory $y(x)$ of the scallop's central sphere, beginning at the disk and ending at the triangle

It is natural to ask how the initial orientation θ_0 affects the scallop's subsequent motion. To investigate this, the simulation was repeated for the initial values $\theta_0 = 0, \pi/3, 2\pi/3$, and π, all other parameters being left unchanged. By symmetry, one expects corresponding motions for negative values of θ_0. Since the vertical motion is that which is interesting, a plot of $y(t)$ for each of these four cases is shown in Figure 5. The case $\theta_0 = \pi/3$, in the second panel, seems to be most successful in generating vertical motion. (In fact, this motivated the choice $\theta_0 = \pi/3$ used throughout the rest of this section.) That this value is the most successful of these four cases may be explained in part by examining the initial configuration of the scallop, depicted in the first panel of Figure 2, in which one of the distal spheres is hanging low, closer to the wall than any of the spheres would be in the cases $\theta_0 = 0, 2\pi/3$, or π. Together with the y^{-3} dependence of the energy (1) by way of equations (2) and (3), this seems to explain why $\theta_0 = \pi/3$ is energetically favorable for vertical motion.

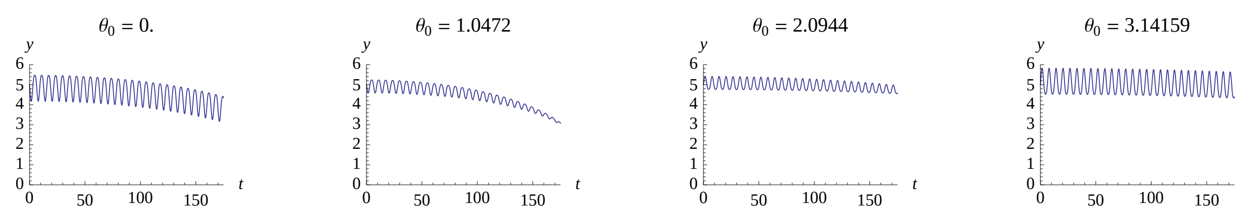

Fig. 5. Vertical position of scallop's central sphere for initial orientations $\theta_0 = 0, \frac{\pi}{3}, \frac{2\pi}{3}, \pi$

4.2. Two-jointed Scallop

The preceding analysis was carried out for the two-jointed scallop depicted in Figure 1. In order that the differences in behavior between the two cases is isolated to the dynamics rather than the choice of parameters, the numerical values for the two-jointed scallop were chosen to agree, insofar as possible, with those in the single-jointed scallop previously considered.

The values of a, l_1, and l_2 chosen satisfy the inequalities (10) imposed on the two-jointed swimmer, so the distal spheres are guaranteed to not collide with each other or with the central sphere. The shape angles

ϕ_1 and ϕ_2 may therefore be actuated arbitrarily. The following open-loop control was utilized, driving the joint angles periodically, although out of phase with one another:

$$\phi_1(t) := \sin(t), \tag{21}$$
$$\phi_2(t) := \sin(t)\cos(t). \tag{22}$$

The resulting gait in shape space is that of a figure eight.

The configuration of the two-jointed scallop at equally spaced time intervals $t = 0, \frac{1}{3}t_{\max}, \frac{2}{3}t_{\max}, t_{\max}$ is depicted in Figure 6. As before, comparison of the leftmost panel ($t = 0$) with the rightmost panel ($t = t_{\max}$) shows that, with some effort, the swimmer inches its way towards the wall. Figure 7 depicts the overall

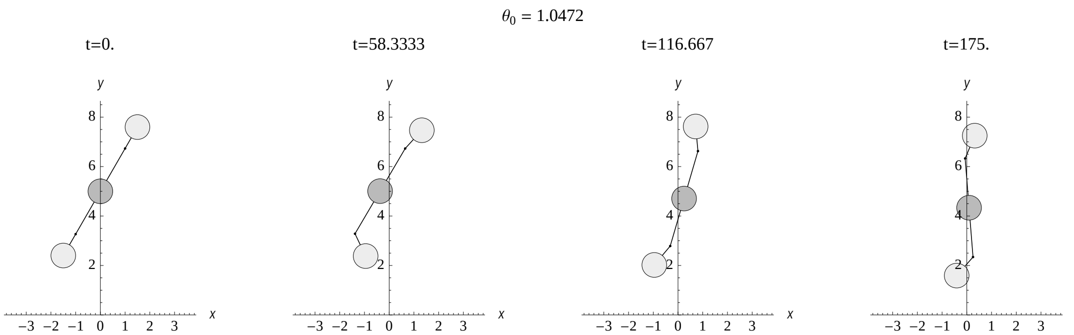

Fig. 6. Snapshots of two-jointed scallop at equally spaced times

orientation of the swimmer. Unlike the case of the single-jointed scallop in Figure 3, the orientation of its two-jointed counterpart is primarily oscillatory, although its average orientation angle does increase over a longer time scale. Finally, the trajectory $y(x)$ is depicted in Figure 8. Its complexity is explained by the fact that two — rather than one — shape variables are present.

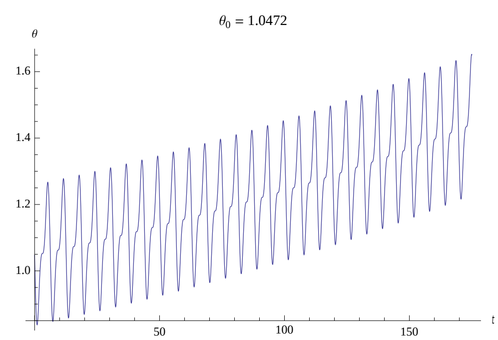

Fig. 7. Orientation of two-jointed scallop

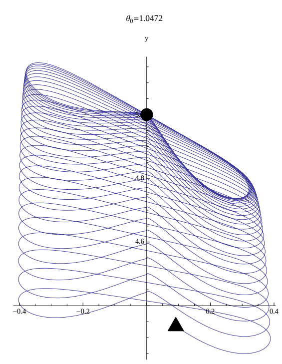

Fig. 8. Trajectory $y(x)$ of the two-jointed scallop's central sphere, beginning at the disk and ending at the triangle

Figure 9 depicts the effect of the initial orientation on the subsequent evolution of $y(t)$, the vertical coordinate of the central sphere. Similar reasoning as in the scallop explains why the initial angle $\theta_0 = \pi/3$ seems to be the most effective of those studied in generating vertical motion. The vertical motion of the two-jointed scallop is somewhat less pronounced than that of the scallop, in part due to the fact that the other distal sphere is further from the wall than in the scallop. Finally, the complicated gait of the two-jointed scallop is reflected by the jagged evolution of $y(t)$ in Figure 9. (Contrast this with $y(t)$ for the scallop, as depicted in Figure 5.)

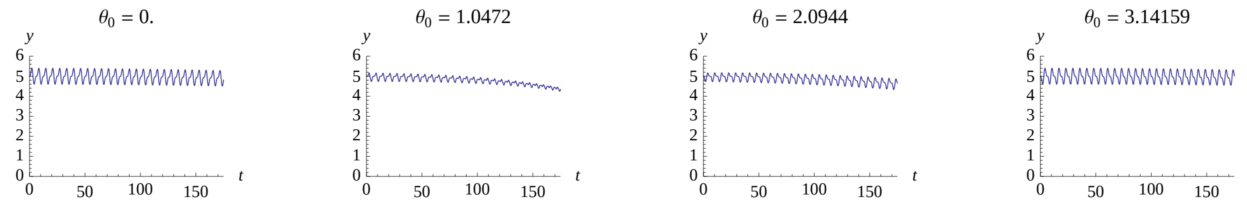

Fig. 9. Vertical position of two-jointed scallop's central sphere for initial orientations $\theta_0 = 0, \frac{\pi}{3}, \frac{2\pi}{3}, \pi$

5. Locomotion and Geometric Phase

Because the Lagrangian is not invariant under vertical translations, trajectories cannot be horizontal with respect to a *mechanical connection* (see (Kelly and Murray, 1995) and (Marsden, 1992)). Nevertheless, it is intriguing to note that the locomotion presented above seems to exhibit qualities consistent with the presence of an underlying geometric phase, in the sense that the final displacement and reorientation resulting from cyclic shape changes is independent of the speed at which those shape changes were executed. To verify this, multiple identical simulations were performed differing only in the time parameterization of the control law. For each value of $\tau \in \{1, 10, 100\}$, the substitution $t \mapsto t/\tau$ was made in the control laws and the maximum simulation time was adjusted to $\tau t_{\max}$. The trajectory and orientation plots for each case is displayed in Figure 10.

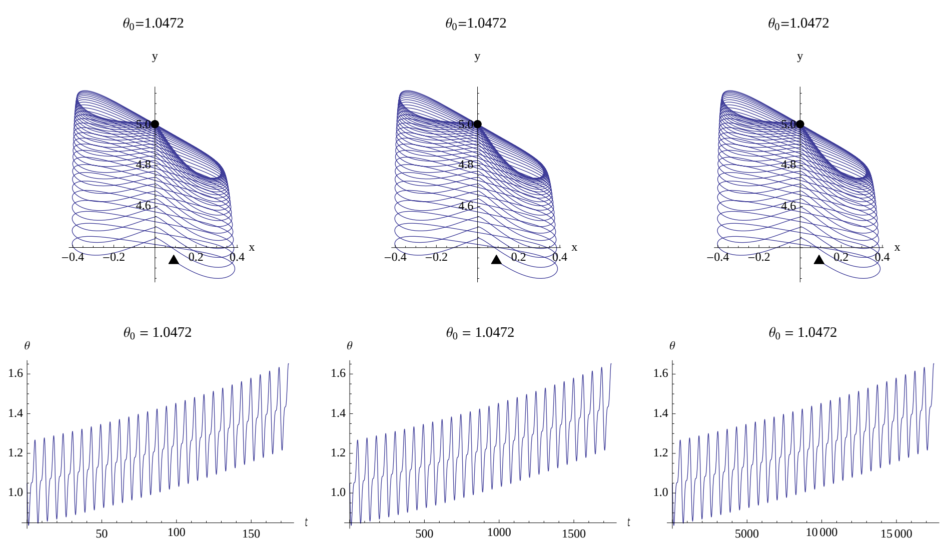

Fig. 10. Evidence for a geometric phase in the two-jointed swimmer
(note the different time scales)

Although this particular procedure represents a linearly scaled reparameterization, it does intriguingly suggest that there may be an interpretation whereby the dynamics are captured by some notion of connection.

6. Conclusions and Future Work

We have demonstrated that the presence of a stationary wall in an ideal fluid can enable the nearby locomotion of a jointed body lacking sufficient shape dependence in its effective inertia to propel itself otherwise. We have observed, furthermore, that while the wall's role is one of symmetry breaking, its presence does not rule out the presence of a geometric phase underlying the body's motion. The following list offers suggestions for possible future work.

- The validity of the hydrodynamic decoupling assumption and the regime in which the approximation (1)-(3) is valid should be investigated.
- Modifying the Lagrangian to account for first-order interactions between the spheres seems advisable, as does including second-order terms describing the interaction of the spheres with the wall.
- Further investigations into the possibility of a geometric phase hinted at in the last section should be performed.
- The phenomenon of *damping-induced self-recovery* was recently discovered in (Chang and Jeon, 2013). The model in this paper includes no viscous effects, and it would be of interest to investigate whether the aforementioned phenomenon would influence the trajectories of the swimmers considered here, if our model were adjusted to accommodate viscous drag.

References

Chang, D. E. and Jeon, S. (2013). Damping-induced self recovery phenomenon in mechanical systems with an unactuated cyclic variable. *ASME Journal of Dynamic Systems, Measurement, and Control*, 135(2).

Kanso, E., Marsden, J. E., Rowley, C. W., and Melli-Huber, J. (2005). Locomotion of articulated bodies in a perfect fluid. *Nonlinear Science*, 15:255–289.

Kelly, S. D. and Murray, R. M. (1995). Geometric phases and robotic locomotion. *Journal of Robotic Systems*, 12(6):417–431.

Kelly, S. D., Pujari, P., and Xiong, H. (2012). *Geometric mechanics, dynamics, and control of fishlike swimming in a planar ideal fluid*. Springer.

Koiller, J., Ehlers, K., and Montgomery, R. (1996). Problems and progress in microswimming. *Journal of Nonlinear Science*, 6(6):507–541.

Marsden, J. E. (1992). *Lectures on Mechanics*. Cambridge University Press.

Milne-Thomson, L. M. (1968). *Theoretical Hydrodynamics, 5th. Ed.* Macmillan.

Purcell, E. M. (1977). Life at low reynolds number. *American Journal of Physics*, 45(3):3–11.

Radford, J. (2003). *Symmetry, Reduction, and Swimming in a Perfect Fluid*. PhD thesis, California Institute of Technology.

Ross, S. D. (2006). Optimal flapping and rowing strokes for self-propulsion in a perfect fluid. *Proc. of 2006 American Control Conference*, pages 4118–4122.